scientific reports

Check for updates

OPEN

Remote sensing of soil moisture using Rydberg atoms and satellite signals of opportunity

Darmindra Arumugam[1]✉, Jun-Hee Park[1], Brook Feyissa[1,2], Jack Bush[1,2] & Srinivas Prasad Mysore Nagaraja[1,2]

Spaceborne radar remote sensing of the earth system is essential to study natural and man-made changes in the ecosystem, water and energy cycles, weather and air quality, sea level, and surface dynamics. A major challenge with current approaches is the lack of broad spectrum tunability due to narrow band microwave electronics, that limit systems to specific science variable retrievals. This results in a significant limitation in studying dynamic coupled earth system processes such as surface and subsurface hydrology from a single compact instrument, where co-located broad spectrum radar remote sensing is needed to sense multiple variables simultaneously or over a short duration. Rydberg atomic sensors are highly sensitive broad-spectrum quantum detectors that can be dynamically tuned to cover micro-to-millimeter waves with no requirement for RF band-specific electronics. Rydberg atomic sensors can use existing transmitted signals such as from navigation and communication satellites to enable remote sensing. We demonstrate remote sensing of soil moisture, an important earth system variable, via ground-based radar reflectometry with Rydberg atomic systems. To do this, we sensitize the atoms to XM satellite radio signals and use signal correlations to demonstrate use of these satellite signals for remote sensing of soil moisture.

Keywords Remote sensing, Rydberg atoms

Remote sensing of the earth system from space relies on a vast network of technologies[1]. Spaceborne radars play a key role for remote sensing applications spanning several science focus areas[2] such as surface, topography, vegetation science[3], or planetary boundary layer science[4]. Major challenges with state-of-art classical radar remote sensors today include band specific RF antennas and RF electronics, lack of tunability, and large form-factors that limit applicability to a specific science objective[2–4]. It is challenging today to develop a single compact instrument that can enable co-located broad-spectrum remote sensing. As a result, many distinct satellite radars covering different bands are needed to study coupled variables of the Earth system such as precipitation and soil moisture, which would require remote sensing covering long-to-short microwave wavelengths (I/P-K bands)[2]. To address this problem, a tunable radar system is needed that does not rely on band-specific microwave electronics.

Radar systems have traditionally required an onboard transmitter and receiver; However, increasingly remote sensing is achieved via use of existing satellite signals referred to as signals of opportunity (SoOp)[5–8], removing the need for an onboard transmitter. Dynamically tunable receivers could use radio reflectometry techniques[9,10] with SoOp signals spanning I-K bands to obtain wide-spectrum responses of the earth system. Downlink satellite radio signals from communication/navigation satellites could permit thousands of active transmissions spread throughout the radio window (VHF-to-K, example 137/260/360 MHz /1.5/2.3/3.9/12.4/18.5/20.7 GHz, see Supplementary Section 1) to be used for remote sensing. However, due to bandwidth limitations in antennas[11] and microwave electronics[12], traditional radio receivers are not practical to cover the entire radio window.

Atomic sensors use highly coherent quantum systems to probe atoms and measure weak signals with high sensitivity or precision[13]. Alkali atoms with high vapor pressure (such as Cesium/Cs and Rubidium/Rb) driven to a high principal quantum number and in the Rydberg states have been shown to be sensitive to microwave-to-millimeter waves[14–16]. Typically, two or more lasers are used to prepare and probe the atoms[15,16] to sense microwave fields, by first creating transparency of the probe laser light via electromagnetically induced transparency (EIT)[17], and then observing the perturbation of the EIT spectrum due to the external microwave fields.

[1]Jet Propulsion Laboratory, California Institute of Technology, Pasadena, CA 91109, USA. [2]These authors contributed equally: Brook Feyissa, Jack Bush and Srinivas Prasad Mysore Nagaraja. ✉email: darmindra.d.arumugam@jpl.nasa.gov

State-of-art techniques with Rydberg atomic systems can detect both amplitude and phase of the incoming microwave field[18] using a local oscillator (LO) to drive the atoms via super-heterodyning[19].

We demonstrate use of Rydberg sensors configured with atomic super-heterodyning to remotely sense soil moisture using XM radio satellite signals (2.320–2.345 GHz). To achieve this, we utilize signal correlators with the use of a direct and reflected signal to extract signals below the atomic readout noise floor and invert the magnitude of the correlator to soil moisture. Although the present work is specific to XM satellite signals and sensing of surface soil moisture, the general approach of using Rydberg atoms opens a pathway to enable broad-spectrum remote sensing of multiple variables of the earth system using thousands of navigation and communications satellite transmissions that cover I-K bands (see Supplementary Section 1).

Results

Correlations to extract modulated signals from noise

Soil moisture retrievals with existing satellite signals are most sensitive to microwave (MW) remote sensing in the P-S band[5] (Supplementary Section 1). We focus on the XM satellite radio band spanning 2.320–2.345 GHz[20]. Figure 1a shows the high-level concept, where SoOp signals reflected of the ground are sensed by a Rydberg atomic sensor and interpreted for soil moisture. Figure 1b shows the quantum optics setup developed for this purpose, which consists of Cesium atoms in a vapor cell at room temperature, laser systems comprised of a probe (~ 852 nm) and tunable coupler (~ 509 nm) laser, and microwave injection system. The probe and coupler are counter-propagated, and a reference probe beam is formed using a beam displacer to reduce or remove technical (phase and amplitude) noise. A transverse electromagnetic (TEM) cell is used to couple MW signals to the vapor cell with high efficiency. The probe and coupler Rabi frequency was set to $\Omega_{p,c}/2\pi = 6.25$ MHz and 0.68 MHz, respectively. The laser wavelengths were used to drive $6S_{1/2}$–$6P_{3/2}$–$66D_{5/2}$, and a strong (− 19 dBm) MW local oscillator (LO) (see Fig. 1)[19] is used to drive to $67P_{3/2}$. The passband of the TEM cell was from DC-3 GHz (< 3 dB insertion loss) (details of experimental setup is presented in Methods).

To sense and retrieve soil moisture from heavily modulated and weak satellite signals, classical SoOp systems utilize signal correlators to extract signals out of the system noise floor[9] (see Supplementary Section 1). A similar approach for signal correlation is needed for the atomic system, because the SoOP signals are expected to be buried in the atomic readout noise (see Supplementary Section 1). We investigate this by injecting a QPSK (quadrature phase shift keying) modulated signal (10 kHz modulation rate) into the TEM/vapor cell and correlate with a copy of the reference waveform (known random bit-stream) with $\Delta f = 50$ MHz (see Fig. 1 and 2). The correlator gain (the processing gain from correlation) is $G_c = BW \times \tau$, where BW is the modulated signal bandwidth, and τ the correlation time. Typical SoOp signal processing approaches are limited by the decorrelation time of the geophysical environment observed, resulting in G_c between 30 and 43 dB (Supplementary Section 1). We estimate the pre-correlation signal-to-noise (SNR) using a 1 Hz resolution bandwidth power spectrum and compare to the post-correlation SNR obtained by peak detection[21]. We find that the correlator output SNR is higher than the pre-correlation SNR by $\sim 10\log_{10} G_c$ (see Supplementary Section 2 for details), and that signals up to this value below the atomic readout noise floor can be extracted with high linearity (Fig. 2b). This demonstrates that weak modulated signals below the atomic readout noise can be extracted via correlation with a known reference waveform by as much as the correlation gain.

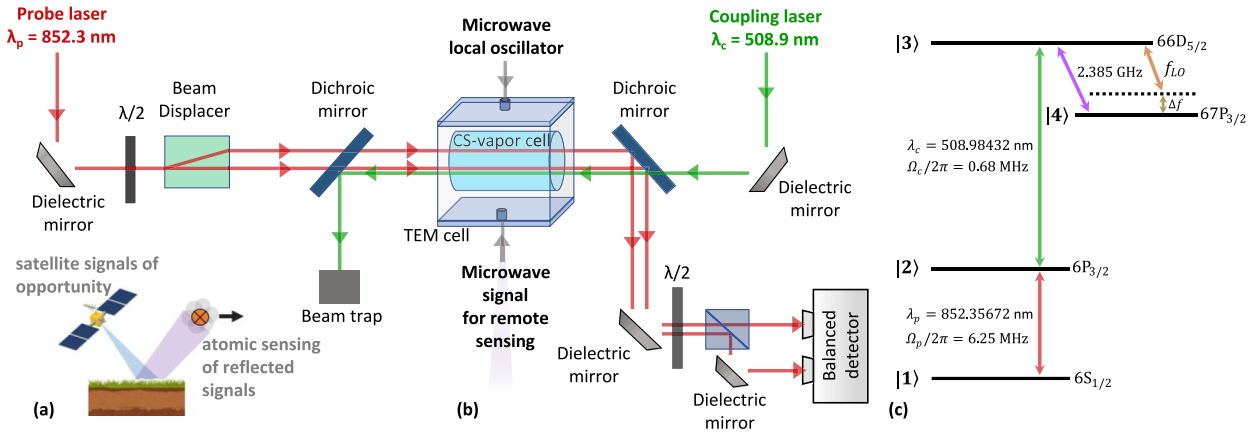

Figure 1. (**a**) High level concept for remote sensing of soil moisture based on reflected satellite signals of opportunity sensed via Rydberg atoms. (**b**) The probe and coupler laser light are counter-propagated in a Cesium vapor cell to excite atoms to the Rydberg state. The vapor cell is located inside a transverse electromagnetic (TEM) cell, which is used for uniform microwave (MW) field coupling to the vapor cell. Both the MW signal to be detected and the local oscillator (LO) field is coupled into the TEM cell. A beam displacer is used to develop a reference probe beam for balanced detection to reduce technical noise. (**c**) The coupler drives the atoms to a principal quantum number of n = 66, and MW signal and LO is off-resonant by about 40–65 MHz from the next nearest state $66D_{5/2}$-$67P_{3/2}$ transition of 2.385 GHz.

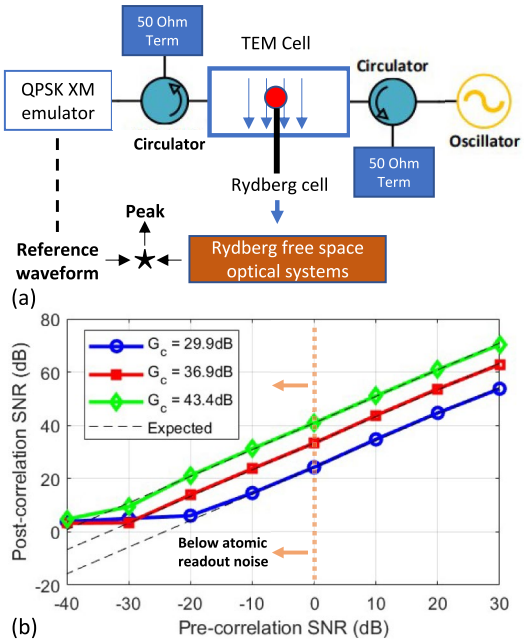

Figure 2. A QPSK (quadrature phase shift key) signal with known bitstream is injected into the TEM/vapor cell to study signal-to-noise (SNR) after correlation with a reference waveform (**a**). The post correlation gains from the atomic readout demonstrated a gain close to the calculated G_c (correlator gain) (by −3 dB) (**b**).

Continuous XM satellite spectral envelop detection

Recent work has demonstrated the first detection of XM satellite signals in a discontinuous spectrum using a Rb Rydberg atomic system[22]. Resonantly (or close to resonant) coupling with Rb systems would require n > 90 and is generally impractical. As a result, the approach required use of a mm-wave (MM) source (119 GHz) to drive the Rb atoms to a high orbital angular momentum, $L > 4$, to sensitize the atom to lower MW frequencies[22]. To avoid high-L, which results in lower sensitivity to MW's and an additional MM source, we use Cs atoms driven to $66D_{5/2}$ that gets close to a resonance ($\Delta f = 40$–65 MHz, see Fig. 1c). The nearest state is $67P_{3/2}$ with a resonance at 2.385 GHz. To continuously detect the entire XM satellite band (2.320–2.345 GHz), we configure a quantum–classical correlator system as shown in Fig. 3. A horn antenna (~ 10 dB gain) is used to couple incoming MW to the TEM/vapor cell via a low noise amplifier (LNA, 31.5 dB gain), bandpass filter, and 12 m or 50 m coaxial RF cable (Fig. 3a). The 12 m coaxial cable was used for all measurements except the natural terrain experiments,

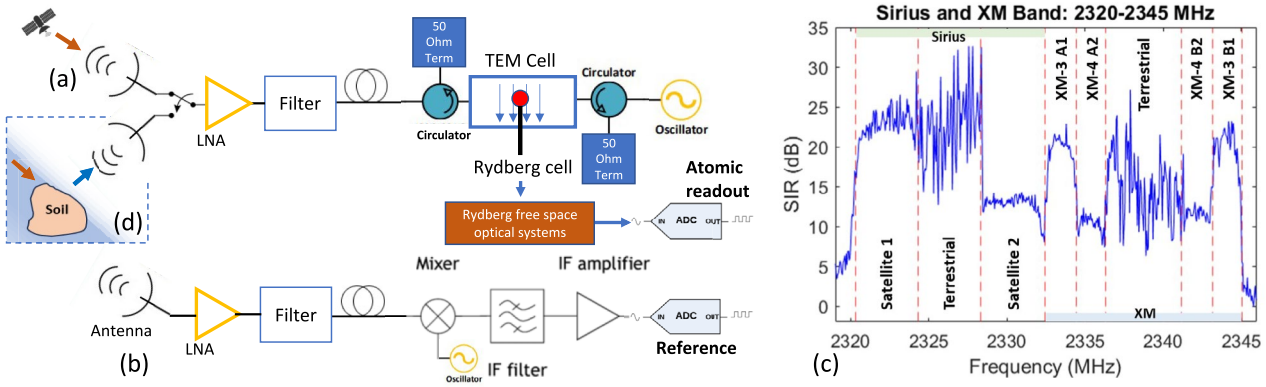

Figure 3. A horn antenna is connected to a low noise amplifier (LNA), then a filter, and a long coaxial cable (50 m long) to drive the atomic system via the TEM cell. (**a**) The horn is pointed towards the XM satellite (see Methods) to detect XM satellite signals. (**b**) A classical system with the same horn, LNA, filter, and coax cable is used to drive an RF mixer, IF (intermediate) filter and amplifier. Both quantum and classical readouts are digitized with an analog-to-digital converter (ADC) and correlated to compute the envelop by sweeping local oscillator frequencies (**c**) Continuos readout of the XM satellite band using the correlations between (**a**, **b**). Both satellite and terrestrial repeaters are sensed. (**d**) The quantum systems (antenna) is directed downward towards the specular reflection to sense reflections off the soil sample (see Methods).

where lengths were 50 m. A reference signal is obtained using the same components (antenna, LNA, filter, long coax) with a RF mixer (LO power of 13dBm with < 6 dB conversion loss), IF (intermediate) filter and amplifier (Fig. 3b). Both quantum and classical (reference) output is digitized by an analog-to-digital convertor (ADC) and correlated similar to Fig. 2. Both channels use a common LO, with attenuators used to set to -19dBm for the Rydberg LO and + 13 dBm for the classical reference LO. LO frequency was swept from 2.319 to 2.346 GHz to readout the entire spectrum via off-resonant Rydberg excitation[23]). Figure 3c shows the output of the correlator after continuously sweeping the LO through the entire band. The result is the entire XM signal spectral envelop to include satellite and terrestrial repeaters. The Sirius satellite occupies the lower 12.5 MHz band with 2 satellite sub-channels (~ 4 MHz bandwidth/channel), while XM occupies the higher 12.5 MHz band with 4 satellite sub-channels (~ 2 MHz bandwidth/channel). We find the correlations to have a signal-to-interference (SIR) of > 10 dB for the satellite signals. We use the term interference, to avoid specific reference to thermal noise as the source of background noise, as we expect background interference to be the key limitation in the present ground experiments near the laboratory. The type of interference is not specifically identified in the measurements. The instantaneous bandwidth (throughout the band) was observed to be about 150 kHz. See Methods for details. We estimate SNR of the detected Sirius Satellite 1 by using a regulated guard band to estimate noise. This data is collected at edge of the Sirius band (Satellite 1, see Fig. 3c), where a regulated guard band (RFI free at 2.3195–2.32 GHz) exists adjacent to this band. This permits a SNR estimation for Satellite 1 over background noise by collecting noise power in the RFI free band (guard band) and comparing to signal power from Satellite 1. We find an estimated SNR from this measurement of about 20.4 dB with the estimated effective bandwidth of 150 kHz and with a signal collected over a 100 ms duration. The effective bandwidth is limited by coupler Rabi frequency and can be increased in future work to > 10 MHz. We further estimate that processing the entire 4 MHz bandwidth of the Sirius Satellite 1 band would result in an additional signal power gain of about 14.26 dB. This would bring the total achievable SNR to about 34.6 dB with the Rydberg ground system configured to process the entire Sirius Satellite 1 sub-channel.

Soil moisture retrievals using emulated XM signals

To study the sensitivity to soil moisture (SM), the system in Fig. 3d was used first in a laboratory environment with an emulated XM QPSK modulated signal (center frequency of 2.333 GHz, 2 MHz bandwidth, with known random bitstream, output power of – 10 dBm, no LNA used, and 12 m cable loss of about 15 dB). A vector signal generator (VSG) was used to generate the emulated signals, which was driven to a transmit antenna (see Fig. 4a, b), while a receive antenna was used to receive the scattered fields off the soil sample. LO frequency was set to 2.333 GHz. Rabi frequencies and LO power was identical to the previous setup. The soil sample was composed of sand (fine, particle size < 0.42 mm) in a 1.5 × 2 × 1.5 feet container. MW absorber foam was used to attenuate the reflections of the edges of the container. An in-situ SM probe was used to obtain ground truth (GT) data. The measurements were collected initially as a dry sample, where average SM GT was 7.95%. Tap water was added to progressively increase the volumetric SM content (VSM) to average values of 14.65%, 21.75%, and visible saturation at 34%. GT measurements were highly variable and repeated to develop error bars in Fig. 4c. Measurements at GT = 34% were normalized relative to scattering coefficient calculations from an integral equation method (I2EM)[24], which enable conversion to scattering coefficients (see Supplementary Section 3). We use a linear radar scattering coefficient to SM model[25] ($\sigma_{soil}^{dB} = \alpha M_v + \beta$, where α is the slope between SM and radar scattering coefficients, β a constant dependent of soil roughness, and M_v the VSM). The surface roughness and incidence angle are static in this experiment. Additionally, the measurement zone is small in scale compared to

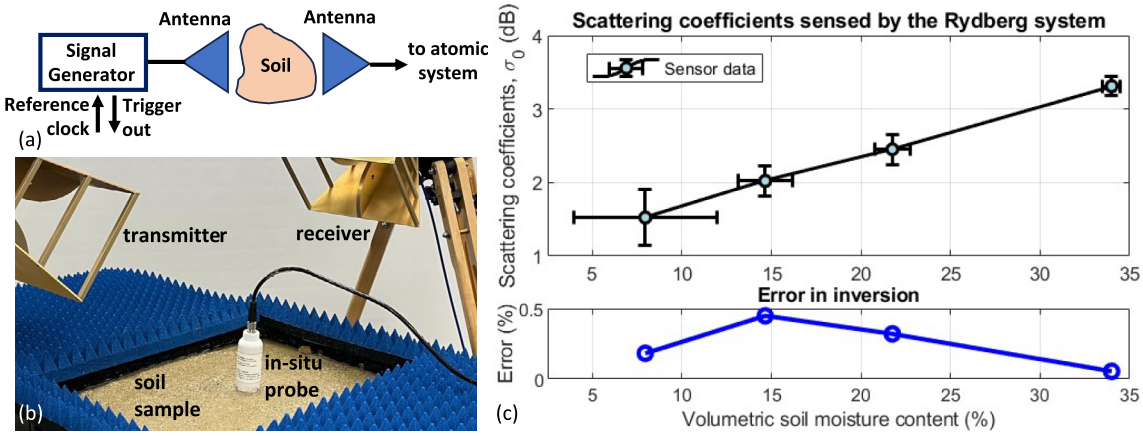

Figure 4. An emulated XM signal (2 MHz bandwidth QPSK signal with random bitstream) is used as a transmitter to study sensitivity of Rydberg atomic detectors to soil moisture (SM). (**a**) The transmitter is driven by a vector signal generator. (**b**) A soil sample (sand, fine particle size < 0.42 mm) is used in a sample container of 1.5 × 2 × 1.5 ft. MW absorber foam is placed outside the specular region to attenuate reflections of the container and ground. An in-situ SM probe is used to obtain ground truth measurements. (**c**) Radar scattering coefficients sensed by the Rydberg atomic readout (top) and error is SM (bottom) inversion as a function of volumetric SM content, showing < 0.5% error in SM inversion (see Methods for details).

spatial inhomogeneity in the soil moisture content (specular Fresnel zone is small). As a result, α and β is found via best fit to data, and the resulting inversion to VSM shows an error < 0.5% (see Fig. 4c) demonstrating effective SM retrieval using the atomic system over the VSM range from 7.95 to 34%.

Soil moisture sensing using XM satellite signals

SM sensing with satellite signals was achieved initially using a similar (container) concept as in Fig. 4 in an outdoor environment to utilize XM satellite signals (see Fig. 5a). The Rydberg readout and reference signal were obtained using the setup in Fig. 3d, b, respectively. The VSM change was induced progressively by adding water, and SM dynamically inverted by correlating the quantum and reference signals and using the linear SM model (see Supplementary Section 3). The GT data was obtained when the sample was dry (5%) and saturated (37%). The system (LO) was tuned to a center frequency 2.333465 GHz, which is the center frequency of the XM-3 A1 sub-channel, and this channel was used for remote sensing of SM. The approach to adding tap water is highlighted in Supplementary Section 3. After each added water (AW) cycle (Fig. 5b), the SM retrievals peak initially due to surface water, then rapidly reduce to steady state SM due to flow of water. The rate of water flow is related to percolation time[26] (or hydraulic conductivity), and an exponential fit of the data after-AW cycles reveal that the percolation time constant increases with each AW cycle up to about > 9 min near saturation (Fig. 5c). (An inverse relationship between hydraulic conductivity and the percolation rate is observed, see Supplementary Section 4).

The same configuration was used in an open outdoor terrain composed of predominantly compacted clay, with the same XM-3 A1 channel for remote sensing. The system was configured to use an additional classical readout as a means of comparing the SM retrievals from the Rydberg system (see Supplementary Section 5 for system details). In this measurement, rapid flow of water was added between 0.2 and 2 min (see Fig. 6) to the

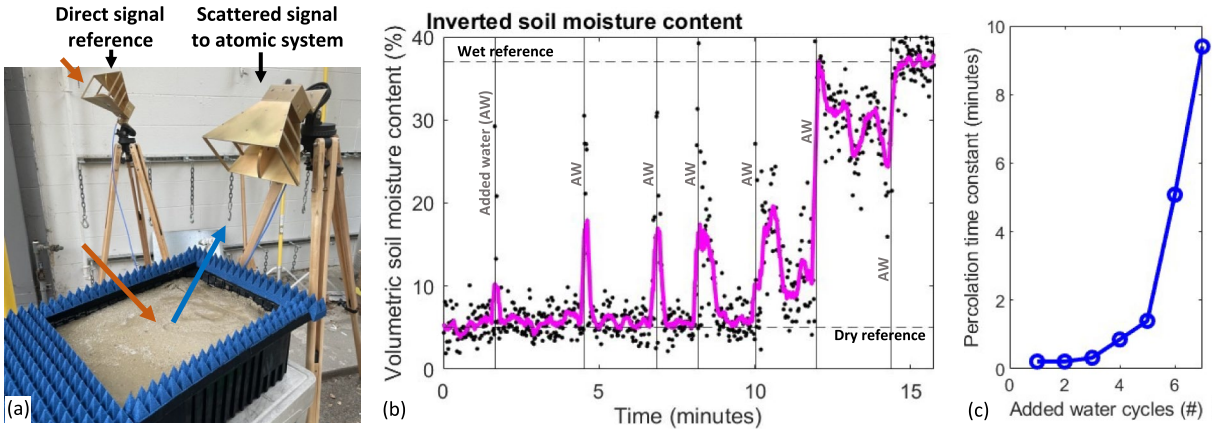

Figure 5. SM sensing using XM satellite signals (XM-3 A1 sub-channel). (**a**) The soil sample was identical to Fig. 4. (**b**) VSM was inverted dynamically based correlations to a reference and using a linear SM model. The solid line is a 10 point moving average (**c**) An exponential fit for data after each added-water (AW) cycle shows a percolation time constant that increases with each cycle to > 9 min.

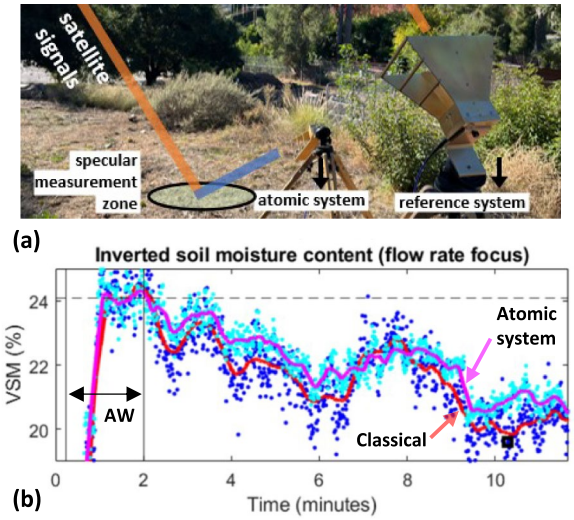

Figure 6. SM sensing in an outdoor natural terrain (**a**) and response to a rapid flow of water (duration < 2 min) with comparison to a classical SM retrieval system (**b**) (detailed figure in Supplementary Section 5).

measurement site, after which the soil was visibly saturated. The measurements were collected for < 15 min to show a slow rate of percolation due to the compacted natural soil. The Rydberg atomic SM retrievals closely matched the classical approach (see Supplementary Section 5 for more details). Due to ground-based measurements, path loss differences for the direct and indirect paths are minimal, and as a result, the ground reflected SIR (see Section: Continuous XM satellite spectral envelop detection) would reduce by approximately the radar scattering losses. We use a forward scattering geometry with negligible losses (see Fig. 4c, estimated via IEM) and estimate the ground reflected SIR to be about 11–26 dB. The sources of noise or interference needs to be further studied and will be addressed in future work.

Discussion

Spaceborne radars play a key role in remote sensing of the earth system to study natural and man-made changes in the ecosystem, water and energy cycles, weather and air quality, sea level, and surface dynamics. Different variables in the earth system (such as soil moisture, precipitation, sea surface heights, etc.) respond to different radar wavelengths or bands spanning micro-to-millimeter waves. As a result, many distinct satellite radars covering different bands are needed today to study coupled variables of the earth system. Rydberg atoms can be sensitized to enable micro-to-millimeter wave detectors that could potentially revolutionize satellite-based remote sensing by enabling a dynamically tunable radar system that does not rely on narrow-band RF electronics. In this work, we demonstrated remote sensing of soil moisture, an important earth science variable, using Rydberg atoms and satellite signals of opportunity. Although the present work is specific to XM satellite signals, the general approach opens the possibility of dynamic broad-spectrum remote sensing via Rydberg atoms by using existing signals of opportunity. To achieve broad-spectrum tunability with Rydberg atoms, narrow-band antennas and filters (presently used) will need to be removed (see Methods, Roadmap to broad-spectrum remote sensing). The tunability (kHz to THz) of Rydberg atomic detectors will enable broad spectrum satellite-based remote sensing for radars and radiometers when effectively coupled to broadband directive elements such as reflectors/focusing dishes.

Methods

Theory for Rydberg readout of QPSK MW

The 4-level super-heterodyning (super-het) is achieved by using a counter propagated probe and coupling laser (see Fig. 1b) and an RF field. The Hamiltonian takes the form[27]:

$$H = \frac{\hbar}{2}\begin{bmatrix} 0 & \Omega_p & 0 & 0 \\ \Omega_p & -2\Delta_p & \Omega_c & 0 \\ 0 & \Omega_c & -2\left(\Delta_p+\Delta_c\right) & \Omega_{RF} \\ 0 & 0 & \Omega_{RF} & -2\left(\Delta_p+\Delta_c+\Delta_{RF}\right) \end{bmatrix},$$

where Δ_p, Δ_c, and Δ_{RF} are the probe, coupler, and MW detuning's, and Ω_p, Ω_c, and Ω_{RF} the Rabi frequencies associated each, respectively. The setup in Fig. 1, uses an on-resonant (close to resonance) probe and coupler, so that $\Delta_{p,c} \approx 0$. The approach to sense MW is via probe laser light spectroscopy from $|1\rangle$ to $|2\rangle$, which is calculated using the density matrix component (ρ_{21}) obtained from the master Eq. [28]:

$$\dot{\rho} = \frac{\partial \rho}{\partial t} = -\frac{i}{\hbar}[H,\rho] + \mathcal{L},$$

where $\mathcal{L}$ is the Lindblad operator for the atoms decay processes. When $\Delta_{RF} \approx 0$ (on-resonance MW), the probe laser light readout gives[19,23], $P_{ON}(t) \propto \langle E_T \rangle_\tau \sim E_{LO}/2 + (E_{MW}/2)\cos(\delta t + \phi_{LO})$, where δ is the difference frequency between the LO and MW RF signals. In the $\Delta_{RF} \neq 0$ off-resonant case (see Fig. 1c), the Stark shift of the optically probed state depends on the atomic polarizability[23]: $\Omega_{OFF} = \alpha E_\tau^2/2$, where α is the polarizability of the state. We use Cs atoms and optically probe $66D_{5/2}$, giving an estimated polarizability of this state[27] of $\alpha = 334.08$ MHz cm^2/V^2. In this off-resonant case:

$$P_{OFF}(t) \propto \langle E_T^2 \rangle_\tau \approx \frac{E_{LO}^2}{2} + E_{MW}E_{LO}\cos(\delta t + \phi_{LO}),$$

where we assume $E_{LO} \gg E_{MW}$, and that $\omega_{MW} \gg \delta$. In this case, the LO field acts as a gain mechanism to the MW field and is optimized to as high a value as possible without saturating the system. In this work, we use QPSK signals (emulated or satellite signals). The signal model for QPSK is given by[21] $s(t) = E_{MW}\cos(\omega_{MW}t + \theta_n)$ within a symbol duration, where $s(t)$ is the QPSK signal, $\theta_n = (2n-1)\pi/4$ with $n = 1, 2, 3, 4$. This implies a high-pass ($\delta > 0$) Rydberg readout with LO phase calibration (set $\phi_{LO} = 0$) given by:

$$S_{OFF}(t) \propto E_{MW}E_{LO}\cos(\delta t + \theta_n),$$

within each symbol rate. The bandwidth of $S_{OFF}(t)$ is limited by the instantaneous bandwidth (IB) of the Rydberg detector which is dependent on primarily the coupler Rabi frequency[29] and is as high as ~10 MHz (empirically demonstrated) or up to ~100 MHz (theoretical shot noise limited). The bandwidth or spectral efficiency of a M-PSK signal is given by $\rho = \log_2 M/2$(bits/s)/Hz, where M is the modulation order. For QPSK signals, the modulation rate is the approximate occupied bandwidth (BW). QPSK signals with modulation rates higher than the Rydberg IB is filtered and limited to the IB.

Theory for correlators

Cross-correlators are used in signal processing to extract the degree of similarity between two signals in reflectometry remote sensing[9,10]. This is based on a sliding dot product between the reference waveform (REF) and the sensed waveform (R, Rydberg readout):

$$\left(f_R \star f_{REF}\right)(T) = \int_{-\infty}^{\infty} f_R^*(t) f_{REF}(t+T)dt,$$

where T is the displacement or lag between the two waveforms. The correlation gain (gain obtained by correlating R and REF) is given by:

$$G_C = BW \times \tau,$$

where it is implied that BW ≤ IB, and τ is the integration time given simply by the duration of the reference and signal. In SoOp approaches, typical correlation gains are $G_c < 45$ dB (example XM-3 A1 signal with sub-channel BW ~ 2 MHz and duration of 1 ms would give $10 \log_{10} BW\tau \sim 33$ dB). For remote sensing on the ground, the delays between REF and R are negligible and $T \sim 0$. After applying a signal correlator, the peak defined by $\left(f_R \star f_{REF}\right)(0)$ gives a measured signal-to-noise (SNR) that is improved relative to the pre-correlation SNR (defined by spectral signal-to-noise estimation at 1 Hz resolution bandwidth) and is given by $10 \log_{10} G_c$ (dB).

Experimental set-up

Multiple experiments were conducted to advance towards satellite based remote sensing of soil moisture. The setup for the Rydberg atomic system was identical in all cases (see Fig. 1). The vapor cell was 7.5 cm in length, quartz construction with 2° angled windows. The vapor pressure at 20 °C was 1.1 μhPa (micro- hectopascals). The 4-level configuration (Fig. 1c) is realized by $6S_{1/2}$–$6P_{3/2}$–$66D_{5/2}$, and a strong (− 19 dBm) MW local oscillator (LO) to drive to $67P_{3/2}$. The two lowest states were $6S_{1/2}$ F = 4 and $6P_{3/2}$ F = 4, driven by the probe laser. The frequency of the probe laser was locked to the hyperfine structure via a standard saturation spectroscopy technique[30], giving a probe wavelength of λ_p ~852.35672 nm. Probe linewidth is estimated to be < 150 kHz. The coupler laser driven to $66D_{5/2}$ was frequency locked using a cylindrical cavity (50 mm diameter × 100 mm length) with finesse of $F_c > 10$ k. the cavity was placed inside a vacuum housing with multiple internal shields to ensure temperature control at the cavity of < 1 mK/day, with a thermal time constant of about 38 h. This is achieved using a cylinder cavity preinstalled in a vacuum housing, and by placement of compact ion pump internally. The ion pump is kept on continuously to reach and maintain pressures < 10^{-6} Torr. The Pound–Drever–Hall (PDH)[31] technique was used to lock the coupler wavelength via the electronic side-band (ESB) technique[32] and to reduce the linewidth of the coupler laser to < 100 Hz. The coupler wavelength was λ_c ~508.98432 nm. Probe power and beam diameter was about 60 μW and 1.1 mm ($1/e^2$ diameter). Coupler power and beam diameter was about 50mW and 1.3 mm. Probe and coupler laser diodes were a commercial external cavity laser diode (ECDL). The coupler at ~ 509 nm was achieved via frequency-doubling (second harmonic generator). The resulting Rabi frequencies were $2\pi \times 6.25$ MHz and $2\pi \times 0.68$ MHz. On-resonance MW frequency was 2.385 GHz to $67P_{3/2}$. For XM detection in the 2.320–2.345 GHz band, the system was off-resonant by Δf = 40–65 MHz. The LO signal was driven at − 19 dBm.

The Cs vapor cell was located inside TEM cell (length: 390 mm, width: 100 mm, height: 62 mm, septum (the conductive strip in the center section) height: 28 mm). The TEM transmission loss up to 3 GHz was < 3 dB. Both MW signal and LO was coupled into opposite directions of the TEM cell (see Fig. 1). A MW circulator (maximum insertion loss < 0.7 dB) was used in either side to isolate the signal and LO by > 18 dB in each direction. MW LO signal was generated by a RF signal generator in CW (continuous wave) mode with a phase noise of about − 66 dBc/Hz at 1 Hz offset. The antenna used for both the atomic and reference (classical) systems were identical, a double ridge guide horn antenna (aperture 13.9 × 24.4 cm, 20.3 cm length), had a gain of about ~ 10 dB over the XM band, and a beamwidth of 30° (H-plane). A coaxial cable of length ~12 m was used for all measurements except the natural terrain experiments, where lengths were ~50 m. The 12 m cables had a loss of < 15 dB (standard coaxial), while the 50 m cables had a loss of < 25 dB (low-loss coaxial cables). The directly coupled QPSK emulated correlation experiment (Fig. 2) and the in-lab SM retrieval via emulated XM signal generation (Fig. 4) did not utilize low-noise-amplifiers (LNA). The other experiments utilized a cascade of two LNA's with gain and noise figures of 11.5 dB and 1 dB, and 20 dB and 1.5 dB, respectively. A bandpass filter with a 2.2–2.4 GHz passband was used after the LNA (when LNA is used), with a pass-band insertion loss of 1 dB and an attenuation of > 20 dB at DC-2 GHz and 2.55–8 GHz. DC blocks were used prior to circulators in either side of the TEM ports to reduce/remove DC biases that may be caused by the RF signal generator (LO generation) or the LNAs (MW signal side). Additional losses of up to 3 dB was measured due to RF connectors and adapters, and cables losses for MW LO was measured at 1.5 dB.

For classical down-converted signals, the signals are obtained using the same components (antenna, LNA, filter, long coax) with an added RF mixer (LO power of 13 dBm with < 6 dB conversion loss), and IF (intermediate) filter and amplifier.

The soil sample used in the container experiments (Fig. 4 and 5) were composed of 100% fine sand particulates with a particle size of < 0.42 mm. The sample container was 1.5 × 2 × 1.5 ft. MW absorber foam was placed outside the specular region to attenuate reflections of the container and ground. The absorber attenuated reflections by > 10 dB at the XM band used in the measurements. Water was added evenly in the using a secondary container to reduce the flow of water via a sparse array of pinholes (container) or a fine column spray (natural terrain). More information on the measurement approach and natural terrain experiment is presented in the Supplementary Section 3 and 5. The in-situ SM probe used was a commercially available handheld RF impedance probe that operated with an CW RF frequency at 50 MHz.

Roadmap to broad-spectrum remote sensing

The present system (see Fig. 3a/d) does not enable broad-spectrum tunability due to use of an antenna and filter. To enable broad-spectrum remote sensing via SoOp, it would be necessary to eliminate classical antenna systems that are generally narrow-band and low-gain. This can most directly be achieved by coupling the vapor cell to a reflector dish without a feed, which focuses the incoming signal into the vapor cell (fields focused directly into the vapor cell, with no requirement for a classical feed) via either its' primary focus or by using a secondary focus such as in Cassegrain or offset secondary reflector[33]. The key advantage of a reflector dish (part of a standard reflector antenna, but without the feed) is that it provides focusing and field enhancements over a broad range of frequencies and is not limited by the narrow-band nature of the feed structure. The atomic resonances will be used to remove strong unwanted emissions at other frequencies. In-band unwanted emissions are filtered in processing using the high spectral resolution (with resolution in kHz due to millisecond signal durations) digital filters, as well as further reduced through correlation filters. The work described in this article is for a ground-based system with XM satellite signals, where Doppler corrections are not needed. A spaceborne system will require Doppler corrections for both direct and indirect signals prior to correlations. This can be done in software (digital Doppler shifting) or by tuning the local oscillators driving each detector to correct shifts. The reflector coupled atomic system will thus have a frequency dependence limited by the reflector (addressed below) and the sensitivity of the atomic detector that is sensitized to various RF bands. Laser tuning is needed to dynamically tune between RF bands, and this can be achieved with commercial tunable diodes (e.g., extended cavity diode lasers) that can readily tune over a > 4 nm range—resulting in RF detection over the MHz to THz range. The sensitivity of the atomic detector at various bands has not been fully characterized and will be the focus of future work. The reflector focusing dish (typically parabolic) can enable beam steering, which is convenient to dynamically alter remote sensing coverage beams and are mature for deployable applications[33]. In addition, parabolic focusing dishes have an upper frequency limited by surface roughness that can extend to millimeter waves[33]. They have a gain of $G_A = e_A(\pi d/\lambda_{MW})^2$, where e_A is the aperture efficiency (which is typically between 0.55 and 0.7, but can reach ~0.9[34]), d the diameter, and λ_{MW} the MW wavelength. As example, a deployable 1 m scale focusing dish with e_A=0.9 and surface roughness < 0.1 mm, would give a gain between 20 and 66 dB (at 2–200 GHz). In addition, techniques for resonators such as the split-ring-resonators[35] can be used to further enhance fields for the low-frequencies ($\lesssim$4 GHz), however methods to integrate these with vapor cells and focusing reflectors are needed. An alternate approach is to advance arrays of Rydberg vapor cell as arrayed detectors[36], however there are considerable challenges in this approach such as coupling laser power requirements growing per node of the array. SoOP processing by a single instrument would be limited by satellite sources of transmissions at different orbital trajectories and locations. The resulting specular reflection locations on the ground would be at different locations for each source at any given instance in time. One approach to offer co-located measurements on the ground is to sequentially sense the satellite signal sources. In this case, as a Rydberg receiver is moving on an orbit, a sequence of specular excitations at the same location on the ground can be used to obtain responses from multiple signal sources. If a reflector is used to focus to a Rydberg cell, then this system would be pointed to the location on the ground using a gimbal or similar. This method of sequential sensing requires coordination or planning to ensure the appropriate signals are sensed. It may be necessary to sense multiple bands simultaneously. The maximum achievable instantaneous bandwidth of the standard Rydberg atomic detector is expected to be up to about 10 MHz[29]. Techniques such as arraying (including within a single vapor cell)[36] and pulsing coupler/probe lasers or using wave-mixing techniques, have been shown to increase the bandwidth to as high as many tens of MHz[37,38], however the upper limit is not known, and future work is needed to constrain this limit. The instantaneous bandwidth of detection can be split-up to detect multiple bands simultaneously. This can be achieved using multiple local oscillator fields to sensitize the atoms to various transitions in the off-resonant atomic spectroscopy configuration. This has been recently demonstrated for detection of 5 bands spread over nearly two decades from 1.7 to 116 GHz[39].

Data availability

The correlated atomic-to-reference readout (correlation power) and inverted (soil moisture) data represented in Figs. 5 and 6 are available as source data. All other data are available upon request. Requests should be sent to the primary corresponding author, Darmindra Arumugam.

Received: 28 February 2024; Accepted: 29 July 2024
Published online: 04 August 2024

References

1. National Research Council. *Earth Science and Applications from Space: National Imperatives for the Next Decade and Beyond* (The National Academies Press, 2007). https://doi.org/10.17226/11820.
2. National Academies of Sciences Engineering and Medicine. *Thriving on Our Changing Planet: A Decadal Strategy for Earth Observation from Space* (The National Academies Press, 2018). https://doi.org/10.17226/24938.
3. Observing Earth's Changing Surface Topography and Vegetation Structure: A Framework for the Decade, NASA, Surface Topography and Vegetation Incubation Study. 210. https://smd-cms.nasa.gov/wpcontent/uploads/2023/06/STV_Study_Report_20210622.pdf.
4. Toward a Global Planetary Boundary Layer Observing System: The NASA PBL Incubation Study Team Report. NASA PBL Incubation Study Team. 134. https://smd-cms.nasa.gov/wpcontent/uploads/2023/05/NASA_PBL_Incubation_Final_Report_2.pdf.
5. Garrison, J. L. *et al*. SNOOPI: Demonstrating P-band reflectometry from orbit. In *2021 IEEE International Geoscience and Remote Sensing Symposium IGARSS* 164–167 (2021). https://doi.org/10.1109/IGARSS47720.2021.9554546
6. Yueh, S. *et al.* A satellite synthetic aperture radar concept using P-band signals of opportunity. *IEEE J. Sel. Top. Appl. Earth Obs. Remote Sens.* **14**, 2796. https://doi.org/10.1109/jstars.2021.3059242 (2021).

7. Balakhder, A. M., Al-Khaldi, M. M. & Johnson, J. T. On the coherency of ocean and land surface specular scattering for GNSS-R and signals of opportunity systems. *IEEE Trans. Geosci. Remote Sens.* **57**(12), 10426. https://doi.org/10.1109/tgrs.2019.2935257 (2019).
8. Ruf, C. S. *et al.* The CYGNSS nanosatellite constellation hurricane mission. In *2012 IEEE International Geoscience and Remote Sensing Symposium* 214–216 (2012). https://doi.org/10.1109/IGARSS.2012.6351600
9. Yu, K. *et al.* Spaceborne GNSS reflectometry. *Remote Sens.* **14**(7), 1605. https://doi.org/10.3390/rs14071605 (2022).
10. Clarizia, M. P. & Ruf, C. S. On the spatial resolution of GNSS reflectometry. *IEEE Geosci. Remote Sens. Lett.* **13**(8), 1064–1068. https://doi.org/10.1109/LGRS.2016.2565380 (2016).
11. Geyi, W. Physical limitations of antenna. *IEEE Trans. Antennas Propag.* **51**(8), 2116–2123. https://doi.org/10.1109/TAP.2003.814754 (2003).
12. Kummerow, C. D. *et al.* Hyperspectral microwave sensors—advantages and limitations. *IEEE J. Sel. Top. Appl. Earth Obs. Remote Sens.* **15**, 764–775. https://doi.org/10.1109/JSTARS.2021.3133382 (2022).
13. Degen, C. L., Reinhard, F. & Cappellaro, P. Quantum sensing. *Rev. Mod. Phys.* **89**, 035002 (2017).
14. Holloway, C. L. *et al.* Broadband Rydberg atom-based electric-field probe for SI-traceable, self-calibrated measurements. *IEEE Trans. Antennas Propag.* **62**, 6169–6182 (2014).
15. Cox, K. C., Meyer, D. H., Fatemi, F. K. & Kunz, P. D. Quantum-limited atomic receiver in the electrically small regime. *Phys. Rev. Lett.* **121**, 110502 (2018).
16. Anderson, D. A., Sapiro, R. E. & Raithel, G. An atomic receiver for AM and FM radio communication. *IEEE Trans. Antennas Propag.* https://doi.org/10.1109/TAP.2020.2987112 (2020).
17. Fleischhauer, M., Imamoglu, A. & Marangos, J. P. Electromagnetically induced transparency: Optics in coherent media. *Rev. Mod. Phys.* **77**(2), 633–673. https://doi.org/10.1103/RevModPhys.77.633 (2005).
18. Simons, M. T., Haddab, A. H., Gordon, J. A. & Holloway, C. L. A Rydberg atom-based mixer: Measuring the phase of a radio frequency wave. *Appl. Phys. Lett.* **114**(11), 114101. https://doi.org/10.1063/1.5088821 (2019).
19. Jing, M. *et al.* Atomic superheterodyne receiver based on microwave-dressed Rydberg spectroscopy. *Nat. Phys.* **16**, 911–915. https://doi.org/10.1038/s41567-020-0918-5 (2020).
20. Michalski, R. A. An overview of the XM satellite radio system. In *Proceedings of 20th AIAA International Communication Satellite Systems Conference and Exhibit* 12–15 (2002).
21. Shah, R., Garrison, J. L. & Grant, M. S. Demonstration of bistatic radar for ocean remote sensing using communication satellite signals. *IEEE Geosci. Remote Sens. Lett.* **9**(4), 619–623. https://doi.org/10.1109/LGRS.2011.2177061 (2012).
22. Elgee, P. K., Hill, J. C., Leblanc, K.-J., Ko, G. D., Kunz, P. D., Meyer, D. H. & Cox, K. C. Satellite radio detection via dual-microwave Rydberg spectroscopy. Preprint at https://arxiv.org/abs/2305.08707
23. Meyer, D. H., Kunz, P. D. & Cox, K. C., Waveguide-coupled rydberg spectrum analyzer from 0 to 20 GHz. *Phys. Rev. Appl.* **15** (2021).
24. Fung, A. K., Liu, W. Y., Chen, K. S. & Tsay, M. K. An improved IEM model for bistatic scattering from rough surfaces. *J. Electromagn. Waves Appl.* **16**(5), 689–702. https://doi.org/10.1163/156939302X01119 (2002).
25. Zribi, M. *et al.* Soil moisture mapping based on ASAR/ENVISAT radar data over a Sahelian region. *Int. J. Remote Sens.* **28**(16), 3547–3565. https://doi.org/10.1080/01431160601009680 (2007).
26. Bethune, M. G., Selle, B. & Wang, Q. J. Understanding and predicting deep percolation under surface irrigation. *Water Resour. Res.* **44**, W12430. https://doi.org/10.1029/2007WR006380 (2008).
27. Holloway, C. L. *et al.* Electric field metrology for SI traceability: Systematic measurement uncertainties in electromagnetically induced transparency in atomic vapor. *J. Appl. Phys.* **121**(23), 233106. https://doi.org/10.1063/1.4984201 (2017).
28. Berman, P. R. & Malinovsky, V. S. *Principles of Laser Spectroscopy and Quantum Optics* (Princeton University Press, 2011).
29. Meyer, D. H., Cox, K. C., Fatemi, F. K. & Kunz, P. D. Digital communication with Rydberg atoms and amplitude-modulated microwave fields. *Appl. Phys. Lett.* **112**(21), 211108. https://doi.org/10.1063/1.5028357 (2018).
30. Spectroscopic instrumentation. In *Laser Spectroscopy*. https://doi.org/10.1007/978-3-540-73418-5_4 (Springer, Berlin, Heidelberg, 2008).
31. Drever, R. W. P. *et al.* Laser phase and frequency stabilization using an optical resonator. *Appl. Phys. B* **31**, 97–105. https://doi.org/10.1007/BF00702605 (1983).
32. Thorpe, J. I., Numata, K. & Livas, J. Laser frequency stabilization and control through offset sideband locking to optical cavities. *Opt. Express* **16**, 15980–15990 (2008).
33. Rao, S., Shafai, L. & Sharma, S. *Handbook of Reflector Antennas and Feed Systems Volume I: Theory and Design of Reflectors* (Artech, 2013).
34. Rao, S., Shafai, L. & Sharma, S. *Handbook of Reflector Antennas and Feed Systems Volume III: Applications of Reflectors* (Artech, 2013).
35. Holloway, C. L. *et al.* Rydberg atom-based field sensing enhancement using a split-ring resonator. *Appl. Phys. Lett.* **120**(20), 204001. https://doi.org/10.1063/5.0088532 (2022).
36. Otto, J. S., Hunter, M. K., Kjærgaard, N. & Deb, A. B. Data capacity scaling of a distributed Rydberg atomic receiver array. *J. Appl. Phys.* **129**(15), 154503. https://doi.org/10.1063/5.0048415 (2021).
37. Sapiro, R. E. *et al.* Time dependence of Rydberg EIT in pulsed optical and RF fields. *J. Phys. B At. Mol. Opt. Phys.* **53**, 094003. https://doi.org/10.1088/1361-6455/ab7426 (2020).
38. Borówka, S. *et al.* Continuous wideband microwave-to-optical converter based on room-temperature Rydberg atoms. *Nat. Photon.* **18**, 32–38. https://doi.org/10.1038/s41566-023-01295-w (2024).
39. Meyer, D. H., Hill, J. C., Kunz, P. D. & Cox, K. C. simultaneous multiband demodulation using a Rydberg atomic sensor. *Phys. Rev. Appl.* **19**, 014025 (2023).

Acknowledgements

We acknowledge discussions with P. Mao and D. Willey. The research was carried out at the Jet Propulsion Laboratory, California Institute of Technology, under a contract with the National Aeronautics and Space Administration (NASA) (80NM0018D0004), through the Instrument Incubator Program's (IIP) Instrument Concept Development (Task Order 80NM0022F0020). We also acknowledge discussions with A. Artusio-Glimpse, N. Prajapati, C. Holloway, and M. Simons at NIST (National Institute of Standards and Technology), and P. Kunz, K. Cox, D. Meyer at ARL (Army Research Laboratory) as part of the NASA IIP Task.

Author contributions

D.A proposed the project. D.A. and J.P configured the quantum systems to include lasers and locking systems. J.P developed the optical setup. D.A., J.B., B.F., and S.P.M.N, developed the RF and SM systems and measurement concepts. D.A. designed the software scripts for data collection and processed the data for the figures. All authors supported data collection efforts. All authors contributed to discussions of the results and the manuscript.

Competing interests
The authors declare no competing interests.

Additional information
Supplementary Information The online version contains supplementary material available at https://doi.org/10.1038/s41598-024-68914-6.

Correspondence and requests for materials should be addressed to D.A.

Reprints and permissions information is available at www.nature.com/reprints.

Publisher's note Springer Nature remains neutral with regard to jurisdictional claims in published maps and institutional affiliations.